Self-Assembly of Macromolecules within Single Topological Defects of Nematic Solvents

JungHyun Noh[a,‡], Wei Cao[b,‡], Hao Sun[b], Yu Yang[a,c], Nathan C. Gianneschi[b,*], and Nicholas L. Abbott[a,*]

[a]School of Chemical and Biomolecular Engineering, Cornell University, Ithaca, New York 14853, United States

[b]Department of Chemistry, Materials Science & Engineering, Biomedical Engineering, Pharmacology, International Institute for Nanotechnology, Simpson Querrey Institute, Chemistry of Life Processes Institute and the Lurie Cancer Center, Northwestern University, Illinois 60208, United States

[c]Department of Chemical and Biological Engineering, University of Wisconsin-Madison, Madison, Wisconsin 53706, United States

ABSTRACT: Solvent-mediated self-assembly of macromolecules has been widely used as a bottom-up strategy for synthesis of nanostructured materials, but most solvents (e.g., water or isotropic organic solvents) provide limited control over the spatial localization and manipulation of individual assemblies. In this study, we use organic solvents with nematic ordering to explore the possibility of programmed assembly of polymers with tailored side-chains within the nanoscopic cores of topological defects of the nematic solvents by developing structure-property relationships. Variation of the side chains of poly(*n*-alkyl acrylates) (alkyl = butyl, hexyl, and dodecyl) revealed that the driving force for partitioning of the polymers into the nanoscopic cores of topological defects formed in nematic 4'-*n*-pentyl-4-biphenylcarbonitrile (5CB) increased with side-chain length, but controlled self-assembly was not observed. Poly(dimethylacrylamide) was found to be soluble in bulk nematic 5CB but did not partition to defects and poly(2-hydroxyethyl acrylate) aggregated in the nematic solvents prior to partitioning to defects. However, poly(2-hydroxyethyl methacrylate) preferentially partitioned into defects above a critical concentration, forming single, well-defined and reversible assemblies (in the absence of aggregation in the bulk phase) at locations defined by the positions of the defects. By synthesizing co-polymers that incorporated anthracene side-chains, photo-crosslinked assemblies with cross-section diameters of 30 ± 5 nm could be generated in and recovered from the defects. Overall, this study provides design parameters for programmed polymer assembly in topological defects of liquid crystalline solvents, including the polymer side chain structure (polarity, flexibility, hydrogen bonding properties), polymer molecular weight, and properties of the main-chain.

INTRODUCTION

The spontaneous self-organization of molecules, from small molecules to macromolecules, is widely established as a versatile bottom-up strategy to prepare tailored nanostructured materials.[1-3] In many cases, formation of nanoscale structure is driven by interactions between the molecular building blocks and a solvent.[4-7] The thermodynamic driving force leading to formation of micellar assemblies of amphiphiles (surfactants) in water, for example, arises from an increase in entropy, achieved as highly ordered water molecules clustered around the aliphatic (non-polar) tails of surfactants are released into the bulk upon micellization (the so-called hydrophobic effect).[8, 9] In turn, the equilibrium molecular architecture of the amphiphile ("packing parameter")[10] captures the role of repulsive headgroup interactions in limiting assembly growth and plays an important part in determining the morphology of amphiphilic assemblies in water (e.g. spherical, vesicular, cylindrical).[6, 11]

In this paper, we move beyond studies of molecular self-assembly in water to explore the use of structured organic solvents to direct assembly processes.[12, 13] While a range of organic solvents have been explored previously for self-assembly, including hydrogen bonding solvents[14, 15] and ionic liquids,[16, 17] here we focus on organic solvents with long-range orientational ordering, so-called nematic solvents. The focus on nematic solvents, which are one of the simplest classes of liquid crystals (LCs, **Figure 1A-B**)[12, 13] is motivated by the observation that they offer the basis of potential strategies for achieving spatial and temporal control of solvent structure,[18, 19] and thus programming of molecular self-assembly,[20, 21] that are not possible with conventional (isotropic) organic solvents. In particular, the study reported in this paper sought to identify new principles for self-assembly of macromolecules based on geometry-induced (i.e., topological) defects in the ordering of nematic solvents. Topological defects form within confined nematic phases when the orientations of the solvent molecules at the confining surfaces cannot be satisfied in the presence of bulk-like nematic order.[12, 13, 22] The resulting frustration leads to the creation of local disordered

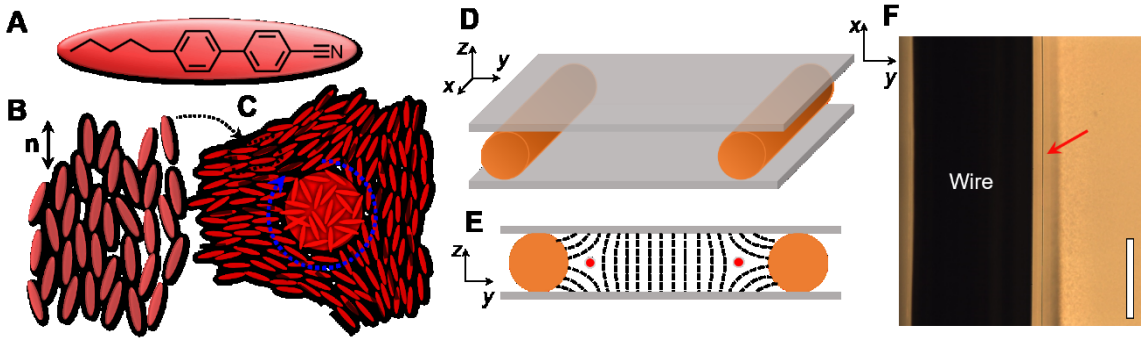

Figure 1. Nematic LCs and disclination lines. (**A**) Molecular structure of 4'-*n*-pentyl-4-biphenylcarbonitrile (5CB). **(B-C**) Schematic illustrations of the orientational order in a nematic solvent and a singular line defect (disclination, oriented towards reader) with strength of $m = -1/2$ (see Results and Discussion for the definition of m and explanation of dotted circular line around the defect core). The black dashed lines indicate the orientations of the mesogens outside the defect core, and the disordered red molecules indicate the core of the defect. For simplicity, the continuous change in ordering between the core and surroundings is not depicted in this illustration. **(D)** Experimental set-up used to generate $m = -1/2$ defects; an optical cell consisting of surface-functionalized copper wires and glass substrates. (**E**) Cross-section of (**D**) in the *yz*-plane, showing a pair of $m = -1/2$ disclinations formed in the confined nematic LC. The dashed lines show local ordering of the mesogens and the red dots represent the cores of the disclinations. (**F**) Bright field optical micrograph of a disclination (indicated by red arrow), formed parallel to the long axis of a copper wire in the *xy*-plane. Scale bar is 200 μm.

regions within the nematic solvent, typically with characteristics dimensions of ~10 nm (for 4'-*n*-pentyl-4-biphenylcarbonitrile, 5CB) at room temperature.[12, 13] Because the equilibrium and dynamic properties of topological defects are well understood in nematic phases,[12, 13] and because topological defects can be formed predictably in a range of system geometries,[23-25] our study tests the hypothesis that topological defects offer the basis of new, versatile and facile ways to control *where and when* molecular assemblies form in a solvent. Specifically, in contrast to formation of molecular assemblies in bulk solvent where the assemblies are mobile (diffuse) and form at random locations,[1, 2, 4-6] topological defects offer the possibility of forming single assemblies at a predictable location within a solvent phase, thus enabling the structure and properties of single molecular assemblies to be studied and exploited: It is this opportunity that motivates the study reported in this paper.

The promise of using defects in nematic solvents for directing the self-assembly of molecules is illustrated by a recent study focused on low molecular weight amphiphiles such as 1,2-dilauroyl-sn-glycero-3-phosphocholine (DLPC).[20, 21] DLPC and related amphiphiles were shown to form organized nanostructures[20, 21] through cooperative processes (a critical aggregation concentration (CAC) was observed) within the solvent environment defined by defects, and under conditions where no measurable association of amphiphiles occurred in the bulk of the phase.[20] The selective assembly of amphiphiles in the defects was proposed to arise, at least in part, from the free energy gain achieved by replacement of disordered, frustrated solvent molecules in the core of the defect by the molecular assembly.[20, 21] Additionally, using experimental values of the CAC, it was determined that the standard free energy of formation of the assemblies was linearly dependent on the tail lengths of the phospholipids.[20] This result is strikingly similar to hydrophobically-driven self-assembly in water where the standard free energy of micellization increases approximately linearly with chain length.[1, 4-5] However, in contrast to water-driven self-assembly, defect-templated self-assembly in nematic solvents allows spatial control over where assemblies form[21] and manipulation of individual assemblies of small molecules amphiphiles.[20, 21]

Whereas the above-mentioned studies of molecular self-assembly in nematic defects focused on small molecule amphiphiles,[20, 21] motivated by the observation that solvent-mediated self-assembly of macromolecules provides access to a broad range of functional nanostructures,[1-3, 7] here we test the hypothesis that defects in nematic solvents can guide the self-assembly of polymers with tailored side-chains into organized nanostructures at well-defined spatial locations. We focus, in particular, on synthetic polymers containing aliphatic side chains. This tests the additional hypothesis that, similar to small molecule amphiphiles, flexible aliphatic chains can be used to tailor solvent-mediated forces that drive self-assembly of polymers within topological defects of nematic solvents. While our results provide support for this hypothesis, in addition, through a series of structure-property studies, we find that the introduction of polar functional groups is necessary to limit further growth of macromolecular assemblies within defects (i.e., to prevent macroscopic phase-separation of the polymers). Here again, we find a strong analogy to self-assembly in water, where polar head-group interactions play a key role in the formation of defined nanostructures.[1, 4, 6]

Finally, as additional context to our study, we note that a large number of past studies have explored polymerization in liquid crystalline (e.g., nematic) solvents to form LC-polymer composites, including in the presence of defect-containing LC phases.[26-32] Our work builds on these past studies by exploring the assembly of preformed polymers in nematic solvents with single defects, with the goal of elucidating structure-property relationships that govern equilibrium self-assembly of the macromolecules. Our approach contrasts to past studies of polymerization in

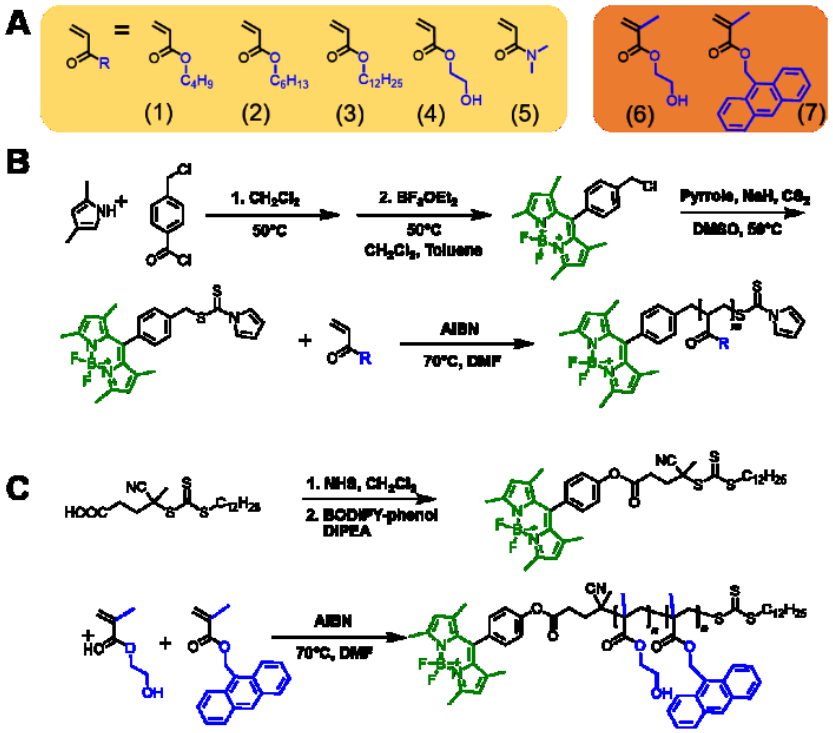

Figure 2. Molecular structures of monomers and synthetic pathways for the preparation of BODIPY-conjugated homopolymers. (**A**) Chemical structures of monomers, containing acrylate or acrylamide (highlighted in yellow box) and methacrylates (red box); **(1)** butyl acrylate, C4; **(2)** hexyl acrylate; C6; **(3)** dodecyl acrylate, C12; **(4)** 2-hydroxyethyl acrylate, HEA; **(5)** dimethylacrylamide, DMA; **(6)** 2-hydroxyethyl methacrylate, HEMA; **(7)** 9-anthracenylmethyl methacrylate, AnMA. (**B-C**) Synthesis of polyacrylate and polyacrylamide (**B**) and (**C**) polymethacrylate via RAFT polymerization. BODIPY fluorophore is highlighted in green. NHS, N-hydroxysuccinimide; DIPEA, N,N-diisopropylethylamine.

Table 1. Polymers used in this study and threshold concentrations for aggregation.

Polymer type	Identifier[a]		DP_m[b]	DP_n[b]	$M_{n,NMR}$ (g/mol)	$M_{n,GPC}$ (g/mol)	$Đ$[c]	Onset of aggregation in defect[d]	Onset of aggregation in bulk nematic solvent[d]
Homopolymers	*n*-alkyl acrylate	C4	103		13.8k	12.9k	1.17	0.15 ± 0.05 μM[e]	7.5 ± 2.5 μM
		C4	50		6.9k	9.0k	1.25	0.4 ± 0.1 μM[e]	
		C4	14		2.3k	N/A	N/A	125 ± 25 μM[e]	
		C6	72		11k	9.2k	1.37	0.25 ± 0.05 μM[e]	
		C6	18		3.3k	2.1k	1.36	7.5 ± 2.5 μM[e]	110 ± 10 μM
		C12	107		26.2k	18.0k	1.47	0.008 ± 0.002 μM[e]	0.075 ± 0.025 μM
		C12	39		9.8k	4.8k	1.34	0.3 ± 0.1 μM[e]	0.8 ± 0.2 μM
		C12	5		1.7k	N/A	N/A	250 ± 50 μM[e]	
	HEMA		90		12.0k	24.5k	1.33	0.045 ± 0.005 μM[f]	0.2 ± 0.1 μM
			50		7.2k	27k	1.30	0.25 ± 0.05 μM[f]	0.65 ± 0.15 μM
	HEA		38		4.9k	12.5k	1.32	No aggregation	0.9 ± 0.1 μM
	DMA		32		3.7k	7.6k	1.32	> 200 μM	> 200 μM
Random copolymers	HEMA-*r*-AnMA		46	18	11.7k	26.8k	1.38	0.45 ± 0.05 μM[f]	0.6 ± 0.1 μM
			22	23	9.9k	13.4k	1.54	No aggregation	> 1.5 ± 0.5 μM

[a]Structures of side chains are shown in **Figure 2A**. [b]Degree of polymerization (DP) for each monomer is indicated by *m* and *n*, as determined by NMR and GPC (see SI for detailed characterization, **Figure S15-S50**). [c]Dispersity ($Đ$) determined by GPC is indicated for each polymer. For N/A, the retention time is too long to calculate M_n and $Đ$ by GPC. [d]Observations were made 30 mins after forming the −1/2 defects. [e]Nucleation and growth in nematic defects leading to uncontrolled growth of micrometer-size polymer-rich domains. [f]Cooperative and reversible self-assembly of well-defined nanostructures in defects.

LCs,[26-32] where consumption of the monomer during polymerization typically involves complex changes in solvent phase behavior, resulting in formation of structures that reflect the kinetics of the polymerization process (not equilibrium self-assembly).[26-32] Although distinct, as detailed later in this paper, we find that results obtained in our studies focused on equilibrium self-assembly provide insights into past observations involving polymerization in LCs containing defects (e.g., so-called blue phase LCs[29-32]). Overall, our study goes beyond past investigations of LC-templated polymerization,[26-32] or self-assembly of polymeric materials in bulk phases,[33, 34] by reporting formation of single assemblies via reversible and cooperative processes involving tailored polymers at topological defects in nematic solvent phases.

EXPERIMENTAL METHODS

Materials. The nematic LC, 4'-*n*-pentyl-4-biphenylcarbonitrile (5CB), was purchased from HCCH (Jiangsu Hecheng Display Technology Co., Ltd). Dimethyloctadecyl[3-trimethoxysilyl)propyl] ammonium chloride (DMOAP), chloroform (HPLC grade) and ethanol (200 proof, HPLC grade) were purchased from Sigma Aldrich (St. Louis, MO). Hexane (HPLC grade, >97.0% (GC)) was purchased from Honeywell Research Chemicals. Deionized water (18.2 MΩ cm resistivity at 25°C) was obtained using a Milli-Q water system (Millipore, Bedford, MA, USA). Fisher Finest Premium Grade glass slides was purchased from Fisher Scientific (Pittsburgh, PA). Copper wire (300 μm in diameter) was obtained from Malin Co. (Brookpark, OH). The AFM tips (triangular in shape, nominal spring constant of 0.03 N m^{-1}) were purchased from Bruker (Camarillo, CA).

Butyl acrylate (C4), hexyl acrylate (C6), dodecyl acrylate (C12), N, N-dimethylacrylamide (DMA), 2-hydroxyethyl acrylate (HEA) were purchased from Sigma Aldrich and purified by passing through a basic Al_2O_3 column to remove the inhibitors. 9-anthrylmethyl methacrylate (AnMA) was purchased from TCI and used as received. 2-Hydroxyethyl methacrylate (HEMA) was purchased from Sigma Aldrich and purified by the following procedure. HEMA was passed through a basic Al_2O_3 column and then dissolved in deionized water. The aqueous solution was then washed with hexanes three times followed by extraction with dichloromethane four times. The dichloromethane layer was combined, and the solvent was removed by evaporation under reduced pressure and then dried in a vacuum desiccator overnight before being transferred to a freezer for further storage. Azobisisobutyronitrile (AIBN) was recrystallized before use. All other chemicals and materials were purchased from Sigma Aldrich and Acros Organics, and used as received unless otherwise stated.

Representative homopolymer synthesis procedure. The acrylate, acrylamide and methacrylate monomers used in our study are shown in **Figure 2A.** We first synthesized a chain transfer agent (CTA) comprising dithiocarbamate that was conjugated to a fluorophore dipyrromethene boron difluoride (BODIPY) via a two-step reaction (**Figure 2B**).[35] The dithiocarbamate CTA was used for polymerization of acrylate monomers; C4, C6, C12, HEA and DMA (**Figure 2A** and **Table 1**). For methacrylate monomers, a trithiocarbonate CTA was designed and synthesized by esterification of a phenol BODIPY with a -COOH bearing trithiocarbonate to match the reactivity of methacrylate monomers (**Figure 2C**).

Reversible addition fragmentation transfer (RAFT) polymerization reactions were carried out under air-free anhydrous conditions in dimethylformamide (DMF) using AIBN as the initiator (**Figure 2B-C**). Specifically, the starting materials were added to a flame-dried Schlenk flask under nitrogen atmosphere. The system was subsequently degassed with three freeze-pump-thaw cycles. Then, the flask was immersed in an oil bath preheated to 70°C and allowed to react overnight under nitrogen. Afterwards, the reaction was quenched by immersion in liquid nitrogen and precipitation by adding cold ether, methanol or hexanes, depending on the solubility of the synthesized polymer. Finally, the polymers were collected by centrifugation and dried under vacuum overnight before use. Additional experimental details and information regarding characterization of the polymers are presented in **Supplementary Information** (**SI**), **Figures S1-S50**. The glass transition temperatures (T_g) of polymers of the type used in our study are also listed in SI (see **Table S1**). We expect, however, that the presence of nematic solvent in our study will substantially influence T_g values.

Preparation of DMOAP-functionalized glass slides and copper wires. A 1% v/v DMOAP solution was prepared by adding 1 mL of 60% v/v DMOAP (dissolved in methanol) into 100 mL deionized water. Glass slides and copper wires were incubated in the DMOAP solution for 2 hours and then sonicated for 10 minutes at room temperature.[36, 37] The glass slides and copper wires were rinsed with deionized water followed by ethanol and dried under a stream of nitrogen gas.

Preparation of mixtures of BODIPY-poly(alkyl acylates) and 5CB. Here we describe the procedure used to prepare a mixture of BODIPY-poly(C4) (DP = 50, 1 μM, equivalent to 0.0006 wt%) in 5CB (**Figure 2A-B** and **Table 1**). The same procedure was used to prepare mixtures of BODIPY-poly(C6) or BODIPY-poly(C12) and 5CB. In brief, 3.45 μL of 0.1 mg mL^{-1} solution of BODIPY-poly(C4) in chloroform was added to 30 μL of chloroform. Then, 50 μL of 5CB was added to the polymer solution. The mixture was placed under vacuum at 45°C for 2 hours to evaporate chloroform. The mixture of polymer and 5CB was kept in the isotropic phase state until it was introduced into the optical cell.

Preparation of mixtures of BODIPY-poly(HEMA/HEA/DMA) and 5CB. Here we describe the procedure used to prepare a mixture of BODIPY-poly(HEMA) (DP = 50, 0.5 μM) in 5CB (**Figure 2A, C** and **Table 1**). The same procedure was used to prepare mixtures of BODIPY-poly(HEA) or BODIPY-poly(DMA) and 5CB. In brief, 1.75 μL of 0.1 mg mL^{-1} of BODIPY-poly(HEMA) in a mixture of chloroform and ethanol (1:1 v/v) was added to 30 μL of chloroform. Then, 50 μL of 5CB was added to the polymer solution. The mixture was subsequently placed under vacuum at 45°C for 2 hours to remove the ethanol and chloroform. The mixture of polymer and 5CB was kept in the isotropic phase until it was introduced into the optical cell.

Fabrication of optical cells. Optical cells were prepared by aligning two DMOAP-functionalized glass slides and spacing them apart with two DMOAP-functionalized copper wires (**Figure 1D, E**). The two surfaces of the cell were glued together using an adhesive (a two-part adhesive consisting of an epoxy resin and polymercaptan and amine curing agents). The mixture of BODIPY-labelled polymer and 5CB in the isotropic phase was introduced into the optical cell and then cooled to the nematic phase at room temperature (21–22°C). Microscopy was performed at 21–22°C.

Fluorescence microscopy of BODIPY-labelled polymers in nematic 5CB. The spatial distribution of BODIPY-labelled polymers in 5CB was imaged by fluorescence microscopy (Olympus IX71, equipped with a mercury lamp). Images were acquired with a Hamamatsu 1394 ORCA-ER CCD camera controlled by Simple PCI imaging software (Compix). The fluorescence filter sets were purchased from Chroma (Bellows Falls, VT). Filter set 1 was used to characterize the monomer signal and consisted of an excitation filter transmitting light at 457-502 nm and emission filter transmitting light at 510-562 nm. Filter set 2 was used to characterize the dimer signal and comprised of an excitation filter transmitting light at 533-584 nm and emission filter transmitting light at 606-684 nm.

Cross-linking of polymers in LC defects. A mixture of photo-crosslinkable polymer (BODIPY-poly(HEMA-r-AnMA), 0.7 μM) in 5CB was prepared using the procedures described above. The anthracene-containing polymer and 5CB mixture in the isotropic phase was injected into the optical cell and then cooled to room temperature. To facilitate the crosslinking of anthracenyl groups, the optical cell was exposed to UV light at 365 nm (EN-280L, Spectroline) for 2 hours. The UV source, with an intensity of 1 mW cm^{-2}, was positioned 5 cm from the sample. We comment here that the cross-linked assemblies did not disassemble upon heating the LC above the nematic-isotropic transition temperature (see **SI, Figure S55**).

Characterization of self-assembled polymeric nanostructures. Prior to performing measurements using scanning electron microscopy (SEM) and atomic force microscopy (AFM), the cross-linked polymeric nanostructures were extracted from the LC defects as follows: 5CB near the cross-linked nanostructure (close to the copper wires in the optical cells, **Figure 1D-F**) was extracted with a micropipette and transferred to the surface of a bare glass microscope slide (we observed the polymeric nanostructures to adhere to the surface of glass). Hexane was added to the 5CB containing the cross-linked structure, and the isotropic mixture of 5CB and hexane was carefully extracted with a micropipette. This process was repeated 5 times to remove 5CB from the substrate. Subsequently, the remaining 5CB and hexane were evaporated under vacuum for 24 hours, leaving only the cross-linked polymeric structures adhered to the glass substrate. The sample was subsequently coated with iridium by sputtering to a thickness of about 5 nm. Imaging of the polymeric assemblies was performed by Zeiss Gemini 500 SEM and operated either at 1 kV or at 5 kV. The same sample (after the coating with metal) was characterized by a Nanoscope IIIa Multimode Atomic Force Microscope (Veeco Metrology Group, Santa Barbara, CA) in contact mode.

RESULTS AND DISCUSSION

As noted in the Introduction, homopolymers were designed, in part, to explore how side-chain structure influences self-assembly in defects (**Figure 2** and **Table 1**). Our hypothesis was that alkyl side-chains can provide the basis of a driving force for partitioning of macromolecules into topological defects of nematic solvents. To test this hypothesis, poly(alkyl acrylates) were synthesized with varying side-chain lengths (alkyl = C4, C6 or C12). Additionally, the degree of polymerization (DP ~ 10, 50 or 100) was varied to investigate the effect of molecular weight on partitioning of polymers into defects. We also synthesized poly(HEA) and poly(DMA) to introduce polar groups (hydroxyl and amide group) into the side-chains and test how interactions mediated by polar groups influence self-assembly in defects. Finally, to investigate the effect of backbone flexibility on the localization of polymers in defects, we compared the behavior of methacrylate and acrylate polymers. Molecular weight and dispersity were determined by NMR and GPC (**SI, Figures S1-S50**).

We employed RAFT to synthesize homopolymers labelled with the fluorophore BODIPY, as shown in **Figure 2**. BODIPY was chosen as the fluorophore because the absorption and emission spectra of BODIPY changes with self-association,[38] thus providing an unambiguous optical signature of the onset of self-association of the homopolymers in 5CB. When BODIPY is singly dispersed in nematic 5CB, absorption and emission occur at 457-502 nm and 510-562 nm, respectively, while association of the fluorophore into dimers results in absorption and emission at 533-584 nm and 606-684 nm, respectively.[20, 21]

Each polymer was dissolved in isotropic 5CB (see **Experimental Methods**) and then the mixture, in the isotropic phase, was introduced into an optical cell (**Figure 1D-F**). The design of the optical cell used to generate defects was similar to that reported previously by Cladis *et al*.[39] In brief, the optical cell was fabricated by placing two copper wires (each with a diameter of 300 μm) between two glass substrates. Both the wires and the glass substrates were chemically functionalized with DMOAP to induce perpendicular anchoring of nematic 5CB at their surfaces.[36, 37, 40-42] These boundary conditions generated two singular disclinations of strength $m = -1/2$ (line defects) after the isotropic phase of 5CB was cooled into the nematic phase. Here we note that defects are classified by defining a charge or strength $m = \pm \alpha/2\pi$, where α is the angle of rotation (in radians) of the LC director **n** when traveling one full rotational circuit around the defect core. As shown in **Figure 1C**, if, upon completing a circuit (indicated by circular dotted line) around the defect core the director rotates by $\alpha = \pi$, the topological strength is $m = -1/2$. The sign of m is determined by whether the director **n** rotates in the same direction (+) or in the opposite direction (–) as the closed path. The $m = -1/2$ defects in our experiments formed parallel to the long axes of the wires (**Figure 1E-F**) and appeared as dark lines in bright-field imaging due to scattering of light. In addition to scattering of light, inspection of **Figure 1F** reveals variation of optical contrast near the defect. This contrast is caused by the change in orientation of the LC near the defect and the associated change in refractive index. We adopted this experimental geometry for the experiments reported in this paper because it leads to the predictable formation of defects that are stable and well-defined in length, allowing for the decoupling of molecular self-assembly from defect dynamics, including any uncontrolled changes in the length of the defect.

Poly(alkyl acrylates). The initial class of polymers that we investigated were poly(alkyl acrylates). Our focus on these polymers (with aliphatic side chains) was motivated by our prior studies of small molecule amphiphiles in which aliphatic tail length was observed to play a key role in triggering self-assembly of the amphiphiles in defects.[20, 21] First, we investigated poly(hexyl acrylate) conjugated to BODIPY (BODIPY-poly(C6), **Figure 2A-B** and **Table 1**) with DP = 18. Both bright field and fluorescence micrographs of –1/2 disclinations in 5CB in the presence of BODIPY-poly(C6) were obtained (**Figure 3**). The images were recorded 30 mins after the isotropic mixtures of 5CB and polymers were quenched into the nematic phase. For concentrations of BODIPY-poly(C6) below 5 μM (DP = 18,

equivalent to 0.005 wt%), we found no measurable difference in the fluorescence signal (both monomer and dimer channels) from the –1/2 disclination and the bulk LC (**Figure 3A-B**). However, when the concentration of BODIPY-poly(C6) was 10 μM, we observed localized bright regions of dimer fluorescence intensity to form along the defect (**Figure 3C**). The dimer signal from the defect was first recorded approximately 15 mins after thermal quenching of 5CB into the nematic phase. However, the monomer fluorescence signal remained similar for both bulk LC and defect. When we increased the concentration of BODIPY-poly(C6) to 75 μM, the number density of bright domains that formed along the defect was found to increase relative to the density observed at 10 μM (**Figure 3D**). Although the dimer fluorescence signal from the defect was intense, the domains were initially too small to be resolved in bright field microscopy, suggesting that the domains are less than a few hundred nanometers in size. However, over time, they grew into micrometer-sized regions that were readily resolved by microscopy (**Figure S53**). Overall, we interpret these results to indicate that BODIPY-poly(C6) partitioned from the bulk LC to the defect to nucleate polymer-rich domains, and that the BODIPY is aggregated within the polymer-rich domains (dimer signal).

Qualitatively similar behaviors were observed for BODIPY-poly(C4) and BODIPY-poly(C12), but a quantitative difference was measured in the concentration of polymer required to observe the onset of nucleation of the polymer-rich domains in the defects. For instance, when comparing BODIPY-poly(C4) and -poly(C6) with similar DP (14 and 18, respectively), the threshold concentration at which nucleation occurred in defects was measured to be about an order of magnitude lower for BODIPY-poly(C6) than BODIPY-poly(C4) (**Table 1**, **Figure 3E**). Although the DP of the two polymers are not identical (14 versus 18), using data in **Figure 3F** (see also **Figure S51**) that show the threshold concentration of BODIPY-poly(C4) as a function of DP (see below for additional discussion), we estimate the threshold concentration of BODIPY-poly(C4) with DP 18 to be 45 μM, which is higher than the threshold concentration of 7.5 ± 2.5 μM for BODIPY-poly(C6) with the same DP. This further supports our conclusion that the aliphatic tail length provides a key part of the driving force for partitioning of polymers into defects. Similarly, when comparing BODIPY-poly(C4) and -poly(C12) with DP (103 and 107, respectively), the threshold concentration was observed to decrease about an order of magnitude for BODIPY-poly(C12) (**Table 1**, **Figure 3E**). This result is generally consistent with a key conclusion emerging from our past studies of the self-assembly small amphiphiles within nematic defects. Namely, that an increase in aliphatic tail length increases the driving force for partitioning of amphiphiles into the defects.

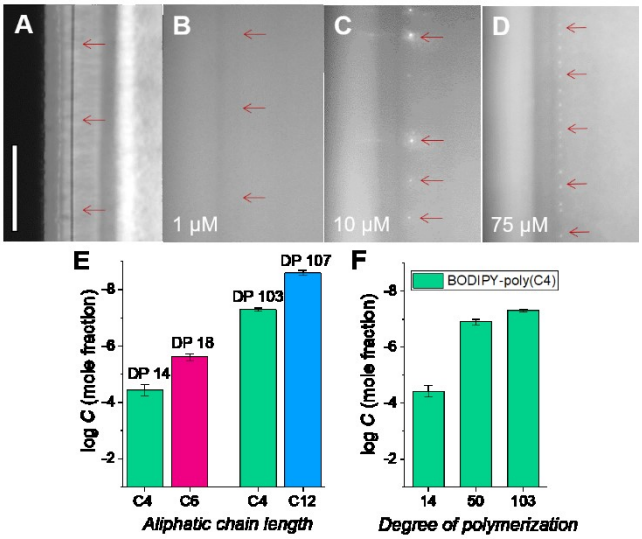

Figure 3. Preferential nucleation of poly(alkyl acrylate)-rich phase at line defects of nematic 5CB. (**A**) Bright field optical micrograph of a singular –1/2 line defect (disclination) and (**B-D**) fluorescence micrographs (λ_{em} = 606-684 nm; dimer signal) showing the localization of BODIPY-poly(C6) (DP = 18) along –1/2 disclination in a nematic solvent. The polymer concentrations are (**A-B**) 1 μM, (**C**) 10 μM and (**D**) 75 μM. Scale bar is 100 μm. (**E-F**) Dependence of threshold concentration (at which nucleation begins), *C*, of poly(alkyl acrylates) on aliphatic tail length (**E**) and (**F**) DP in LC defects. In (**E**), the DPs were similar for C4 and C6, and for C4 and C12. Error bars represent the standard deviation of three experiments.

We also examined the influence of the DP on partitioning of the poly(alkyl acrylates) into the topological defects. When DP was increased from 14, 50, to 103 for BODIPY-poly(C4), the threshold concentrations at which domain formation in defects were observed were found to decrease from 125 μM to 0.15 μM (**Figure 3F**). This result also indicates that as the number of aliphatic side chains on a polymer increases, there is an increase in driving force for nucleation of the polymer-rich phase in the defects. Finally, with increasing DP, the fluorescence signal from the polymer-rich domains changed from being dominated by dimers to arising largely from monomers. This result is consistent with a decrease in the local number density of BODIPY fluorophores in the polymer-rich domains (i.e., dilution) with increase in DP (**Figure S52**).

Overall, the results above reveal that BODIPY-poly(alkyl acrylates) preferentially segregate to defects with a driving force that increases with the aliphatic side chain length. This observation supports our initial hypothesis, formulated from the behaviors of small molecule amphiphiles, that the aliphatic side-chains of the polymers play a key role in driving the polymers to defect cores. However, while our results show that BODIPY-poly(alkyl acrylates) partition to nematic defects, we also conclude that they do not form controlled assemblies. The polymer-rich domains continue to grow and coalesce over time into micrometer-scale droplets of non-uniform size that decorate the defect (**Figure 3** and **Figure S53**). This observation contrasts with past studies on the self-assembly of small amphiphiles in defects,[20, 21] which resulted in formation of stable nanostructures with well-defined morphologies and sizes. Accordingly, we conclude that BODIPY-poly(alkyl acrylates) are not self-assembling in defects but rather than they are forming

polymer-rich phases through a pathway that involves nucleation in the defects.

Poly(HEMA). To prevent macroscopic phase separation, and achieve control over the size of self-assembled structures, we hypothesized that not only is it necessary to have a driving force for aggregation, as provided by the aliphatic chains of BODIPY-poly(alkyl acrylates), but also to introduce a free energy penalty that limits the size of the assemblies formed.[5, 6] This concept underlies ideas such as the "packing parameter" used to rationalize self-assembly of small molecules.[10] Specifically, charge or dipolar interactions between adjacent head groups within an assembly define a preferred spacing between the head groups, which in combination with the structure of the tail, defines a packing parameter.[43] Consistent with this general understanding of self-assembly, we observed previously that self-assembled nanostructures of photopolymerized phospholipids exhibit a multilamellar internal organization when assembled within defects of nematic phases, consistent with dipolar interactions of the zwitterionic head groups of the amphiphiles.[20, 21] Motivated by the general idea that interactions between polar groups may introduce additional constraints on the nanostructure and growth of assemblies of polymers in defects, we next explored the behaviors of polymers that displayed size chains with hydroxyl (poly(HEMA) and poly(HEA)) or amide (poly(DMA)) groups. Below we focus on results obtained with poly(HEMA) because it displayed key signatures of self-assembly in defects, and then briefly compare poly(HEMA) to poly(HEA) and poly(DMA).

BODIPY-poly(HEMA) (**Figure 2C**) presents side chains that end in hydroxyl groups and thus can participate in interactions such as hydrogen bonding with other BODIPY-poly(HEMA) side chains or with 5CB. We dissolved BODIPY-poly(HEMA) with DP = 50 in isotropic 5CB and subsequently cooled the solvent to form –1/2 disclinations (**Figure 4**). When the concentration of BODIPY-poly(HEMA) was below 0.2 μM in nematic 5CB, we measured no significant difference in either monomer and dimer fluorescence intensity between the defect and the bulk LC (**Figure 4A-C**), indicating that the polymer was dispersed uniformly in the nematic solvent. At a concentration of 0.3 μM or higher, the monomer fluorescence signal from the BODIPY-poly(HEMA) abruptly increased uniformly along the defect (**Figure 4E** and **4H**) while the dimer fluorescence signal was indistinguishable from the bulk LC (**Figure 4F** and **4I**). These observations were made 30 mins after forming the –1/2 defects. However, in contrast to BODIPY-poly(alkyl acrylates), the uniform intensity of monomer fluorescence emitted from the defect did change with time and did not transform into a droplet or other non-uniform morphology (observations carried out for one week). These initial observations suggest that the BODIPY-poly(HEMA) assembly formed in the defect is an equilibrium or kinetically trapped structure. Additionally, we did not observe aggregation of the polymer in the bulk of the LC under these conditions.

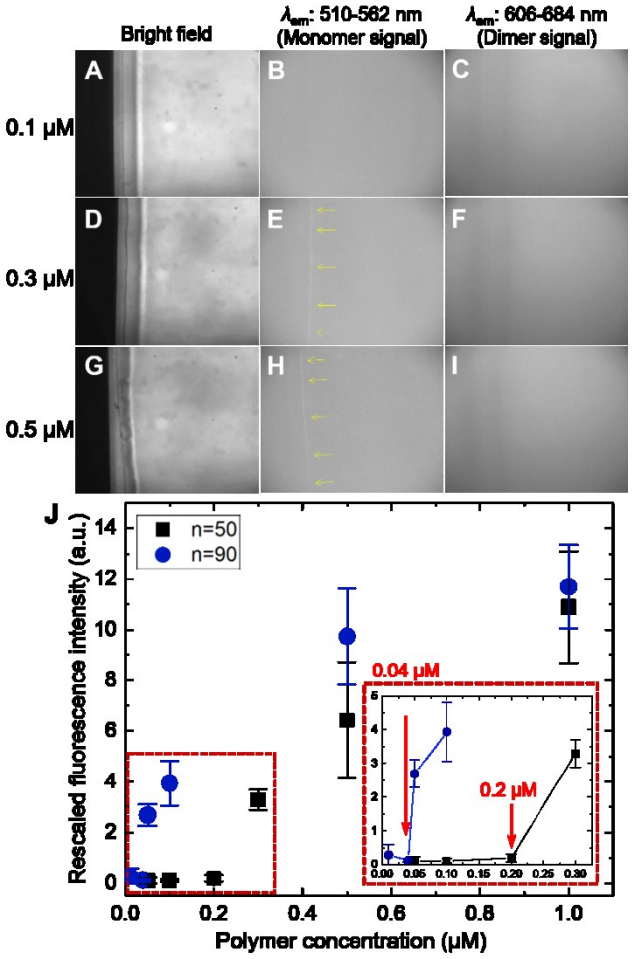

Figure 4. Self-assembly of BODIPY-poly(HEMA) in the nanoscopic cores of topological defects formed in nematic solvents. (**A, D, G**) Bright field micrographs of –1/2 disclinations and (**B-C, E-F, H-I**) fluorescence micrographs (**B, E, H**: λ_{em} = 510-562 nm as monomer signal; **C, F, I**: λ_{em} = 606-684 nm as dimer signal), showing the distribution of the polymers (DP = 50) in the defect-containing nematic solvents. (**J**) Fluorescence intensity (of monomer signal) of BODIPY-poly(HEMA) with DP = 50 and DP = 90 in nematic defects. Inset in (**J**) shows data in the concentration range of 0 – 0.33 μM. The red arrows indicate the concentrations at which assembly begins in the defects.

Quantitative analysis revealed that the monomer fluorescence signal generated by BODIPY-poly(HEMA) (DP = 50) assembled in the defect increased with the polymer concentration above 0.2 μM (CAC, 0.25 ± 0.05 μM; **Table 1** and **Figure 4J**). Moreover, the plot of fluorescence intensity versus polymer concentration reveals the presence of a CAC, consistent with a cooperative association of BODIPY-poly(HEMA) within nematic defects. Similar qualitative behavior was observed with BODIPY-poly(HEMA) (DP = 90), but the threshold concentration was lowered to 0.04 μM (CAC = 0.045 ± 0.005 μM, **Table 1** and **Figure 4J**). This effect of DP is similar to that shown in **Figure 3** with the BODIPY-poly(alkyl acrylates) where higher molecular weight polymers exhibit a larger driving force for partitioning into defects.

For concentrations of BODIPY-poly(HEMA) (DP = 50) above 0.65 μM, we observed aggregation of the polymer in the bulk of the LC phase (**Figure S54**). However, the fluorescence signal from bulk aggregates differed from the defect-templated

assemblies of the BODIPY-poly(HEMA). As noted above, monomer but not the dimer fluorescence signal was generated by assemblies of BODIPY-poly(HEMA) in defects. In contrast, we measured bulk aggregates of BODIPY-poly(HEMA) to generate fluorescence in both dimer and monomer channels. This result suggests that the internal structure of the BODIPY-poly(HEMA) assembly formed in the defect differs from the aggregates that form in the bulk LC. We interpret the absence of dimer fluorescence from the defect-templated assembly of BODIPY-poly(HEMA) to indicate that the assembly formed in the defect has a well-defined internal organization (order) that prevents BODIPY groups covalently attached to one end of each poly(HEMA) molecule from aggregating (and thus generating dimer fluorescence). This finding is similar to that reported previously with the self-assembly of small molecule amphiphiles in defects. When the fraction of amphiphiles labeled with BODIPY was comparable to the BODIPY to polymer repeat unit ratio (e.g., 1:52) used in our study of poly(HEMA), monomer signal only was generated by the BODIPY (in contrast, when every small molecule amphiphile was labeled with BODIPY, dimer fluorescence was observed).[20] We end by noting that our observations with BODIPY-poly(HEMA) contrast to those made with BODIPY-poly(alkyl acrylates) (for similar DPs), for which polymer-rich domains formed in defects and bulk LC generated both dimer and monomer signals (**Figure S52**).

In our previous studies with small molecule amphiphiles, measurements of fluorescence intensity revealed that the defects are saturated by amphiphile at high concentrations.[20] In contrast, inspection of **Figure 4J** does not show evidence of saturation of the defect by polymer over the accessible concentration range. As noted above, however, the low solubility of poly(HEMA) in bulk nematic solvent prevented experiments from being performed at higher concentrations of poly(HEMA).

Formation of an ordered assembly, when driven by thermodynamics, requires reversibility during the assembly process to eliminate incorrectly assembled structures.[6, 44, 45] We examined whether or not the assemblies formed by BODIPY-poly(HEMA) formed reversibly in defects. Sequential images were acquired during heating of 5CB from 22°C (nematic solvent) to 40°C (isotropic solvent) (**Figure 5**). The nematic to isotropic phase transition at 35°C eliminates the disclination, and immediately we observed the assembly of BODIPY-poly(HEMA) break into small aggregates (**Figure 5A-C**). This initial disruption of the assembly likely reflects mechanical stresses imposed on the assembly during the phase transition of the nematic LC to an isotropic oil, as the phase transition generates convection within the 5CB phase. Subsequent observation of the fragments reveals them to dissolve into the isotropic 5CB over 26 hours (**Figure 5D**). The dissolution process was accompanied by an increase in the intensity of monomer signal in the bulk isotropic 5CB. Overall, these observations lead us to conclude that the self-assembly of BODIPY-poly(HEMA) in −1/2 defects of 5CB is reversible.

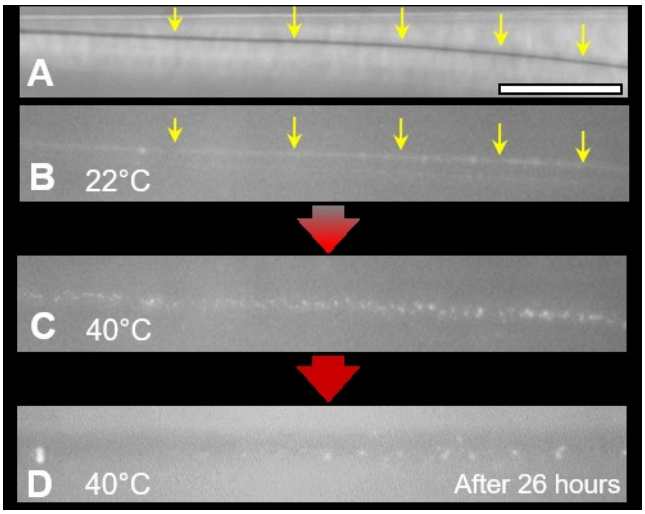

Figure 5. Reversible formation of molecular assemblies of BODIPY-poly(HEMA) templated by topological defects in nematic solvents. (A) Bright field and (B-D) fluorescence micrographs (λ_{em} = 510-562 nm; monomer signal) showing the dissolution of the polymer after heating the nematic solvent (B) at 22°C to an isotropic solvent (C-D) at 40°C. Yellow arrows in (A-B) indicate the location of the defect and the corresponding assembly. Scale bar is 100 μm.

To provide additional insight into the nanostructure of BODIPY-poly(HEMA) assemblies formed in –1/2 defects of 5CB, we sought to form assemblies from related polymers with side chains that can be photo-crosslinked, and then extract and characterize the assemblies post-crosslinking. Specifically, we synthesized the random copolymer BODIPY-poly(HEMA-*r*-AnMA) that incorporated the anthracenyl monomer, AnMA (**Figure 1C** and **Table 1**). We chose AnMA to match the reactivity of HEMA, a methacrylate, and to provide side chains that can be cross-linked by UV exposure. Past studies have shown that anthracene will undergo a [4π+4π] cycloaddition upon UV exposure.[46] We confirmed the photodimerization of anthracene in BODIPY-poly(HEMA-*r*-AnMA) by monitoring the decrease of the π-π* absorption at 368 nm in DMF using UV-Vis spectroscopy (**Figure S47**).

We found that BODIPY-poly($HEMA_{46}$-*r*-$AnMA_{18}$), (where the subscripted number indicates DP of a monomer incorporated into the polymer (randomly)) selectively self-assembled within –1/2 defects of 5CB above a CAC (**Figure S55**). However, the presence of the anthracenyl monomer within the copolymer was observed to cause the CAC of the polymer to increase relative to BODIPY-poly(HEMA) of comparable DP. For example, the CAC of poly($HEMA_{46}$-*r*-$AnMA_{18}$) was measured to be 0.45 ± 0.05 μM (**Table 1** and **Figure S55**), which is 2.5 time higher than that of BODIPY-poly(HEMA) with DP = 50 (0.25 ± 0.05 μM; **Figure 4**). In addition, when the ratio of HEMA and AnMA was 1:1 with BODIPY-poly($HEMA_{22}$-*r*-$AnMA_{23}$), we did not observe self-assembly up to a concentration of 1 μM (**Figure S56**). Above 1.5 μM, we observed aggregates to form in bulk LC with sizes of tens of micrometers, indicating that the solubility limit of the polymer was exceeded in the bulk LC solvent.

Guided by the results above, we assembled BODIPY-poly($HEMA_{46}$-*r*-$AnMA_{18}$) in LC defects (confirmed by fluorescence signature), exposed the defect to UV light, and then heated the nematic solvent above the clearing temperature to

eliminate the defect. When the defect was eliminated by heating to 40°C, the cross-linked assembly did not fragment but rather a contiguous structure was observed to be suspended in isotropic 5CB (**Figure 6A** and **Figure S57**). This result contrasts to the experiment where the assembly of BODIPY-poly(HEMA) fragmented then dissolved upon heating of the 5CB from the nematic to isotropic phase (**Figure 5**).

To transfer the cross-linked polymeric assembly from the isotropic 5CB phase (**Figure 6A**) to the surface of a solid for SEM and AFM, we used a pipette to withdraw the isotropic 5CB containing the cross-linked assembly from the optical cell and deposit it onto the surface of a glass microscope slide. As detailed in **Experimental Methods**, adoption of this procedure was guided by the observation that the polymeric assemblies adsorbed to the surface of the microscope slide (see below). While we were able to use fluorescence imaging (acquisition times of about 2 seconds) to observe assemblies of BODIPY-poly(HEMA$_{46}$-*r*-AnMA$_{18}$) form within LC defects at concentrations of the polymer of ~0.5 μM (**Figure 4** and **Figure S55**), after transfer of the assembly to the surface of the microscope slide, we were no longer able to localize the assembly by fluorescence imaging (even by using long acquisition time).[20, 21] However, by using higher concentrations of BODIPY-poly(HEMA$_{46}$-*r*-AnMA$_{18}$), specifically concentrations above which aggregation of the polymer also occurred in the bulk 5CB, we found that attachment of bulk aggregates to the polymeric assembly formed in the defect provided an effective although crude method to identify the location of the defect-templated assembly on the glass microscope slide for imaging by SEM and AFM. Although we were not able to image the assembly formed in the defect using SEM and AFM in the absence of attachment of bulk aggregates to the polymeric assembly, our observations based on fluorescence microscopy (**Figure 4**) provide support for the formation of assemblies within defects in the absence of bulk aggregates.

Both imaging methods led to identification of worm-like polymeric assemblies that had lengths greater than 10 μm (**Figure 6B-G**). As noted above, the worm-like assembly, which was readily identified due to its uniformity in width, was decorated by disordered polymer aggregates that formed in the bulk of the LC and attached to the assembly formed in the defect. In many images, we observed the defect-templated polymeric assembly to pass under, and extend for 10's of micrometers on either side of the aggregates formed in the bulk LC (**Figure 6** and **Figure S58-S59**). We characterized the widths of the defect-templated polymeric assemblies using three independent samples. We measured the widths at multiple places along each assembly by SEM and calculated the mean and standard deviations to be 33 ± 3 nm, 30 ± 6 nm, and 27 ± 3 nm, respectively. The uniformity in the thicknesses of the nanofibers is consistent with controlled growth of the assemblies within the defects (more images in **Figure S60**). We also used AFM to characterize the nanofibers (same samples used to SEM). While AFM confirmed the uniformity of width, convolution of the AFM tip shape with the nanofiber leads to an overestimate of the nanofiber diameters (the apparent diameters measured by AFM were 136 ± 19 nm, 148 ± 29 nm, and 123 ± 10 nm, respectively).[47] The radius of curvature of the AFM tip used in our study was 30 nm, which is larger than radius of nanofiber (radius of 15 nm, as determined by SEM). As detailed in **SI** (**Figure S61**), we calculated that convolution of the AFM tip shape (radius of 30 nm) with the topography of the nanofiber (diameter of 30 nm) to generate an apparent nanofiber diameter of 120 nm, which is in good agreement with the average of the above-reported experimentally determined values (135 nm ± 20 nm).

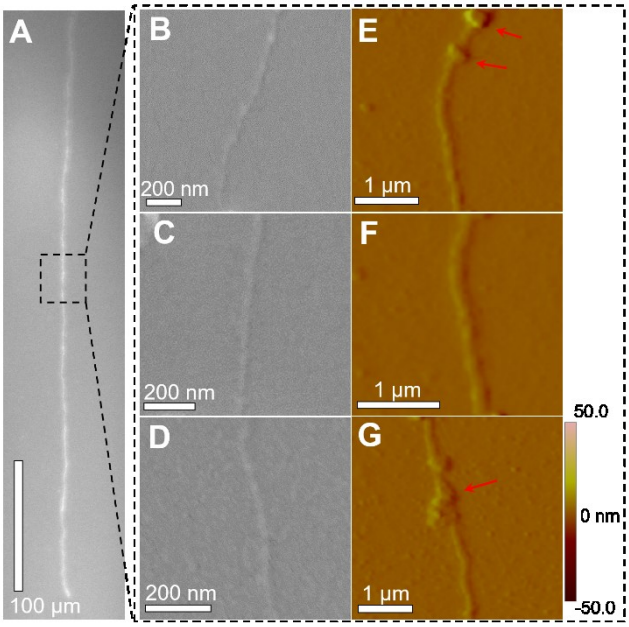

Figure 6. Structure of assemblies of BODIPY-poly(HEMA$_{46}$-*r*-AnMA$_{18}$) formed in *m* = –1/2 topological defects of 5CB and preserved by photo-crosslinking. The concentration of polymer in the 5CB sample was 0.7 μM. (**A**) Fluorescence micrograph of a cross-linked assembly suspended in isotropic 5CB. (**B-D**) Representative SEM and (**E-G**) AFM images of cross-linked assemblies of BODIPY-poly(HEMA$_{46}$-*r*-AnMA$_{18}$) transferred to the surface of glass substrates. Red arrows point to aggregates formed in bulk nematic 5CB that attach to the nanofiber, and were used to identify the locations of the nanofibers on the glass substrates (see text for details).

Poly(HEA). To provide additional insight into the factors that underlie the self-assembly of BODIPY-poly(HEMA) in LC topological defects, we explored the behavior of BODIPY-poly(HEA). BODIPY-poly(HEMA) and BODIPY-poly(HEA) are similar in that both possesses a hydroxyethyl side chain but differ by replacement of the methyl group on the backbone of BODIPY-poly(HEMA) with a hydrogen. In contrast to BODIPY-poly(HEMA), we found that BODIPY-poly(HEA) (DP = 38) did not self-assemble within –1/2 defects of 5CB. Instead, we observed the polymer to aggregate in the bulk nematic 5CB at concentrations of 0.9 μM and above (**Figure 7A-C**). The aggregates that formed in the bulk were observed to partition to the defect, as seen in fluorescence micrographs obtained using the monomer signal (indicated by red arrows in **Figure 7B**). Dimer fluorescence signal was also obtained when imaging the aggregates (**Figure 7C**). This suggests that the internal structures of the aggregates are not well defined, in contrast to the self-assembled structures formed by BODIPY-poly(HEMA) in defects (**Figure 4**).

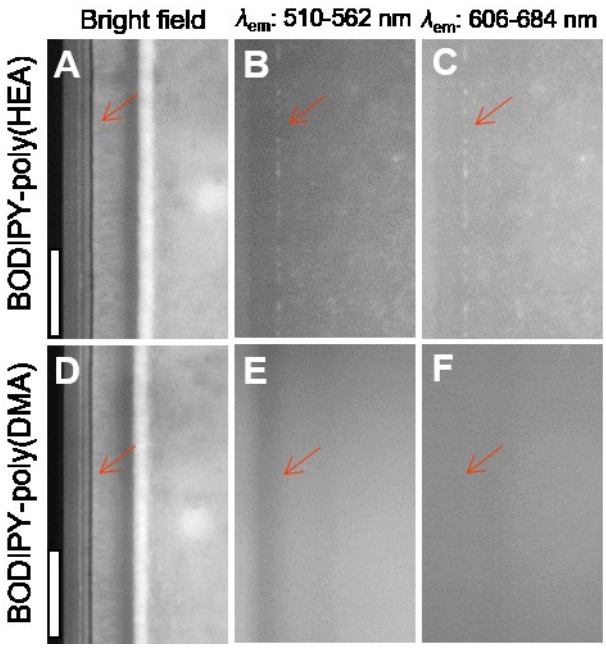

Figure 7. (**A-C**) Aggregation of BODIPY-poly(HEA) (DP = 38) at 1 μM in nematic 5CB. (**D-F**) Dissolution of BODIPY-poly(DMA) (DP = 32) at 1 μM in nematic 5CB. (**A, D**) Bright field and (**B-C, E-F**) fluorescence micrographs; (**B, E**) with monomeric (λ_{em} = 510-562 nm) and (**C, F**) dimeric signals (λ_{em} = 606-684 nm), showing the distribution of polymers in the nematic 5CB. Red arrows indicate the locations of defects. Scale bars are 100 μm.

A key conclusion of our experiment with BODIPY-poly(HEA) is that substitution of the backbone methyl group by a hydrogen has a substantial influence on self-assembly in –1/2 defects, even though the solubility of BODIPY-poly(HEA) in bulk nematic 5CB (1 μM) is comparable to BODIPY-poly(HEMA) (0.65 μM) (for similar DP ~ 40-50). Specifically, at concentrations of polymer between 0.2 μM and 0.65 μM, neither BODIPY-poly(HEA) or BODIPY-poly(HEMA) form aggregates in the bulk 5CB yet poly(HEMA) forms assemblies in the –1/2 defect whereas poly(HEA) does not. Past studies have established that the methyl group of the HEMA reduces rotational degrees of freedom along the backbone of the polymer, leading to an increase in the persistence length of the polymer (**Figure 1A, C**).[48-50] These past conclusions, when combined with our observations, suggest that polymer main-chain flexibility (which impacts the presentation of hydroxyl side chains) impacts that ability of the molecules to self-associate within defects.

Poly(DMA). The final polymer that we examined was BODIPY-poly(DMA) with DP = 32 (**Figure 1A-B** and **Table 1**). The amide group of BODIPY-poly(DMA) possesses a large dipole moment (e.g. dimethylacetamide, 3.79 D).[51] We found this polymer to exhibit exceptionally high solubility in nematic solvents compared to the other polymers used in our study. At concentrations up to 200 μM, we detected no sign of aggregation of the polymer in defects or bulk LC (no dimer signal); the monomer fluorescent signal intensity increased monotonically over the concentration range studied (**Figure 7D-F**, **Figure S62**). These results suggest that the amide group of BODIPY-poly(DMA) interacts favorably with 5CB in the nematic phase, eliminating any driving force for aggregation within bulk 5CB or within a –1/2 defect formed in 5CB.

The structure-property relationships extracted from our experiments suggest that side chain structure (length of aliphatic side chain; presentation of polar and hydrogen bonding functional groups), polymer molecular weight and main chain backbone properties (e.g., conformational degrees of freedom) can influence the self-assembly of polymers in the nanoscopic solvent environment created by topological defects of nematic LCs. In particular, our measurements performed with poly(*n*-alkyl acrylates) revealed the driving force for the partitioning of polymers to defects, resulting in nucleation of polymer-rich phases, to increase with length of the aliphatic side chains of the polymers (**Figure 3E**). Past studies have reported that the solubilities of *n*-alkanes are lower in nematic solvents than isotropic solvents, and that solubilities in nematic solvents further decrease with increase in aliphatic chain length.[52] These effects have been attributed to constraints on the conformational degrees of freedom accessible to the flexible aliphatic chains in nematic solvents.[52] Our results suggest that similar considerations likely underlie the side chain-length dependence of the partitioning of poly(*n*-alkyl acrylates) into defects. We interpret our results with the poly(*n*-alkyl acrylates) to correspond to defect-nucleated phase transitions of polymer-rich phases from nematic solvents that are supersaturated with polymers.

A second key result is that poly(HEA) and poly(HEMA) behave in strikingly different ways in nematic defects in that poly(HEMA) self-assembles and poly(HEA) does not. One possible interpretation of our experiments with poly(HEA) and poly(HEMA) is that main-chain flexibility plays an important role in self-assembly in defects (as poly(HEMA) is less flexible than poly(HEA)[48-50]) and more so than solubility in bulk LC as the solubilities of two polymers in bulk LC were similar. It is also possible that the reduced rotational degrees of freedom along the main-chain of poly(HEMA) places constraints on the configurations of the polymers within assemblies formed in defects, thus promoting the formation of assemblies with organized internal structures and well-defined dimensions (**Figure 6**).

The structure-property relationships obtained in our study reveal that polarity and hydrogen bonding properties of the side chains of the polymers play a key role in self-assembly in nematic 5CB. Similar to the self-assembly of small molecule amphiphiles in water, we interpret results obtained with BODIPY-poly(DMA) to indicate that side chains with sufficient affinity for the nematic 5CB solvent (amide) prevent self-association both in the bulk nematic phase and defects. However, with BODIPY-poly(HEMA), the side-chain polarity prevents aggregation in bulk nematic 5CB at concentrations for which the polymer partitions into –1/2 defects. In comparison to BODIPY-poly(alkyl acrylates), which do not present side-chains terminated in polar groups, growth of assemblies formed by BODIPY-poly(HEMA) within the –1/2 defect was controlled. We attribute the controlled growth of the BODIPY-poly(HEMA) assemblies within the defects to the introductions of interactions between the terminal hydroxyl groups of the polymer side-chains.

Overall, several aspects of our results obtained with BODIPY-poly(HEMA) are similar to past studies of the self-assembly of small molecules in LC defects.[20, 21] In particular, our measurements with BODIPY-poly(HEMA) reveal (i) the presence of a cooperative process of self-assembly in the –1/2

defect, as characterized by a CAC, (ii) reversibility of the self-assembly process, and (iii) controlled growth of the assembly in the defect, as evidenced by the uniform width in of the nanofibers templated from the defects. Additionally, the diameter of the self-assembled structure formed by poly(HEMA-*r*-AnMA) in the –1/2 defect (~30 nm) is comparable to that obtained via self-assembly of phospholipids (~20 nm).

Past studies have extensively explored polymerization in liquid crystalline solvents.[19, 26-32] Of particular relevance to our study are prior investigations of polymerization in LC phases that contain defects, such as blue phase LCs. Past experimental and theoretical studies have reported stabilization of blue phases (i.e., expansion of the range of temperatures over which the blue phase is stable), and attributed the stabilization to segregation of polymers or colloidal particles to disclinations within the blue phase.[29, 31, 53-55] In particular, Kikuchi[31] reported that polymerization of monomers containing flexible alkyl side-chains led to stabilization of the blue phase whereas polymerization of liquid crystalline monomers has a much weaker impact on thermal stabilization. The results that we have obtained with poly(alkyl acrylates) suggest that prior observations of the effectiveness of polymers with flexible side chains in stabilizing blue phases likely reflect the strong tendency of flexible side chains to partition into the core of the defects. More broadly, the structure-property relationships revealed in our study may offer the basis of rational design principles for optimization of polymer compositions for tuning the thermal stabilization of defect-rich LC phases.

CONCLUSIONS

This paper reports structure-property relationships revealing that polymers can undergo cooperative self-assembly processes in the nanoscopic cores of topological defects designed into nematic solvents. In contrast to past studies of polymer self-assembly in isotropic solvents, the defects introduced into nematic solvent structure permit precise control over where within a solvent phase the polymer assemblies form. Defect-triggered assembly also permits formation of single polymeric assemblies within a solvent phase, thus enabling future studies of the properties of single assemblies or the use of single assemblies as functional materials (e.g., conduits for transport processes). We identify key structural features of the polymers that determine whether or not self-assembly is observed, including the polymer side chain structure (polarity, flexibility, hydrogen bonding properties), polymer molecular weight, and properties of the main-chain (constraints on configurational degrees of freedom). In particular, we find that BODIPY-poly(HEMA) exhibits key features of self-assembly (cooperativity and reversibility) in –1/2 defects of nematic 5CB, forming nanofibers with well-defined diameters (30 ± 5 nm) that are comparable in size to the diameters of the defect cores.

Our results also generate a range of important questions for future investigation. Although we have established that the nanofibers templated from the –1/2 defects possess well-defined diameters, we do not yet know how BODIPY-poly(HEMA) is organized within the nanofibers. Additionally, in the current paper, all experiments were performed at room temperature. In future studies, using 5CB at a temperature closer to the nematic-to-isotropic phase transition, where the defect core size is expected to be larger, we aim to determine if the diameter of the assembly templated from the defect can be tuned. Our results also suggest that there exist substantial opportunities to explore additional classes of fluorophores and polymers. For example, we found the level of labeling of the polymers (one end-attached BODIPY) to be insufficient to permit imaging of dried and cross-linked polymeric assemblies. The incorporation of multiple BODIPY groups into each polymer or use of alternative fluorophores should enable this challenge to be addressed. Finally, our results with poly(HEA) and poly(HEMA) suggest that main-chain flexibility is important, but additional studies with polymers that differ systematically in flexibility are needed to further test this proposal. More broadly, this result suggests that self-assembly of polymers in defects of nematic solvents likely reflects a complex balance of entropic and enthalpic contributions to the free energy of assembly formation (analogous to self-assembly in water). This interplay of entropic and enthalpic factors remains to be fully elucidated.

Beyond the open questions identified above for future study, our results reveal many new directions of inquiry. For example, there exist many opportunities to change the architecture of the polymers used for self-assembly in topological defects, including use of block copolymers, bottle-brush polymers and dendrimers. Additionally, the observations reported in this paper are limited to –1/2 line defects in 5CB, and the extent to which similar self-assembly behaviors are observed in other type of defects (e.g., point defects with varying strength) remains an open topic. Finally, we comment that our observations in this paper focus on equilibrium behaviors. In future studies, it would be interesting to determine if defect dynamics can generate morphological changes in the polymer assemblies hosted by the defect. Overall, the findings reported in our paper advance our understanding of key factors that influence molecular assembly of polymers in topological defects of LCs. More broadly, this study highlights the opportunity that exists to generate polymeric nanostructures using LC defects as programmable nanotemplates for directed assembly and synthesis.

ASSOCIATED CONTENT

Supporting Information.
This material is available free of charge via the Internet at http://pubs.acs.org.

Characterization of BODIPY-CTA by ^{1}H NMR, ^{13}C NMR, ^{19}F NMR, ^{11}B NMR and UV-Vis spectra; Characterization of BODIPY-conjugated polymers, including ^{1}H NMR spectra and GPC plot of BODIPY-poly(C4/C6/C12),BODIPY-poly(HEMA/HEA/DMA), BODIPY-poly(HEMA-*r*-AnMA); additional optical micrographs; additional SEM images; calculation of overestimated width caused by convolution effects in AFM.

AUTHOR INFORMATION

Corresponding Author

Nathan C. Gianneschi - Department of Chemistry, Materials Science & Engineering, Biomedical Engineering, Pharmacology, International Institute for Nanotechnology, Simpson Querrey Institute, Chemistry of Life Processes Institute and the Lurie Cancer Center, Northwestern University, Illinois 60208, United States; Email: nathan.gianneschi@northwestern.edu
Nicholas L. Abbott - School of Chemical and Biomolecular Engineering, Cornell University, Ithaca, New York 14853, United States; Email: nabbott@cornell.edu

Author Contributions

The manuscript was written through contributions of all authors. All authors have given approval to the final version of the manuscript. ‡ J.N. and W.C. contributed equally.

Notes

The authors declare no competing financial interest.

ACKNOWLEDGMENT

This research was primarily supported by the Army Research Office (W911NF-15-1-0568 and W911NF-19-1-0071), with additional support from the National Science Foundation (CBET-1803409 and CBET-1852379). Use of the shared facilities of the Cornell Center for Materials Research (MRSEC DMR-1719875) is acknowledged.

REFERENCES

(1) Holmberg, K.; Jonsson, B.; Kronberg, B.; Lindman, B. *Surfactants and Polymers in Aqueous Solution*.; John Wiley & Sons, Ltd.: Chichester, **2003**; pp 1-545.

(2) Alexandridis, P. L.; Lindman, B. *Amphiphilic Block Copolymers: Self-Assembly and Applications*.; Elsevier: Amsterdam, **2000**; pp 1-448.

(3) Hartgerink, J. D.; Beniash, E.; Stupp, S. I. Self-Assembly and Mineralization of Peptide-Amphiphile Nanofibers. *Science* **2001**, *294*, 1684-1688.

(4) Huck, W. T. S. *Nanoscale Assembly: Chemical Techniques*.; Springer: Boston, **2005**; pp 1- 244.

(5) Israelachvili, J. N.; Mitchell, D. J.; Ninham, B. W. Theory of Self-Assembly of Hydrocarbon Amphiphiles into Micelles and Bilayers. *J. Chem. Soc., Faraday Trans. 2* **1976**, *72*, 1525-1568.

(6) Lee, Y. S. Self-Assembly and Nanotechnology: *A Force Balance Approach.*; John Wiley & Sons, Inc.: New jersey, **2008**; pp 1-344.

(7) Wang, Y.; Xu, H.; Zhang, X. Tuning the Amphiphilicity of Building Blocks: Controlled Self-Assembly and Disassembly for Functional Supramolecular Materials. *Adv. Mater.* **2009**, *21*, 2849-2864.

(8) Chandler, D. Interfaces and The Driving Force of Hydrophobic Assembly. *Nature* **2005**, *437*, 640-647.

(9) Huang, D. M.; Chandler, D. The Hydrophobic Effect and The Influence of Solute-Solvent Attractions. *J. Phys. Chem. B* **2002**, *106*, 2047-2053.

(10) Nagarajan, R. Molecular Packing Parameter and Surfactant Self-Assembly: The Neglected Role of the Surfactant Tail. *Langmuir* **2002**, *18*, 31-38.

(11) Pelesko, J. A. *Self Assembly: The Science of Things That Put Themselves Together.*; CRC Press Taylor & Francis Group: Florida, **2007**; pp 1-336.

(12) de Gennes, P. G.; Prost, J. *The Physics of Liquid Crystals.*; Clarendon Press: Oxford, **1993**; pp 1-594.

(13) Kleman, M.; Lavrentovich, O. D. *Soft Matter Physics: An Introduction.*; Springer: New York, **2003**; pp 1-637.

(14) Hunter, C. A. Quantifying Intermolecular Interactions: Guidelines for the Molecular Recognition Toolbox. *Angew. Chem. Int. Ed.* **2004**, *43*, 5310-5324.

(15) Corradi, E.; Meille, S. V.; Messina, M. T.; Metrangolo, P.; Resnati, G. Halogen Bonding versus Hydrogen Bonding in Driving Self-Assembly Processes. *Angew. Chem. Int. Ed.* **2000**, *39*, 1782-1786.

(16) Greaves, T. L.; Drummond, C. J. Ionic Liquids as Amphiphile Self-Assembly Media. *Chem. Soc. Rev.*, **2008**, *37*, 1709-1726.

(17) He, Y.; Li, Z.; Simone, P.; Lodge, T. P. Self-Assembly of Block Copolymer Micelles in an Ionic Liquid. *J. Am. Chem. Soc.* **2006**, *128*, 2745-2750.

(18) Bukusoglu, E.; Bedolla Pantoja, M.; Mushenheim, P. C.; Wang, X.; Abbott, N. L. Design of Responsive and Active (Soft) Materials Using Liquid Crystals. *Annu. Rev. Chem. Biomol. Eng.* **2016**, *7*, 163-96.

(19) Kim, Y. K.; Noh, J.; Nayani, K.; Abbott, N. L. Soft Matter from Liquid Crystals. *Soft Matter* **2019**, *15*, 6913-6929.

(20) Wang, X.; Miller, D. S.; Bukusoglu, E.; de Pablo, J. J.; Abbott, N. L. Topological Defects in Liquid Crystals as Templates for Molecular Self-Assembly. *Nat. Mater.* **2016**, *15*, 106-112.

(21) Wang, X.; Kim, Y. K.; Bukusoglu, E.; Zhang, B.; Miller, D. S.; Abbott, N. L. Experimental Insights into the Nanostructure of the Cores of Topological Defects in Liquid Crystals. *Phys. Rev. Lett.* **2016**, *116*, 147801.

(22) Mottram, N. J.; Sluckin, T. J. Defect-Induced Melting in Nematic Liquid Crystals. *Liq. Cryst.* **2000**, *27*, 1301-1304.

(23) Gu, Y.; Abbott, N. L. Observation of Saturn-Ring Defects around Solid Microspheres in Nematic Liquid Crystals. *Phys. Rev. Lett.* **2000**, *85*, 4719-4722.

(24) Tkalec, U.; Ravnik, M.; Copar, S.; Zumer, S.; Musevic, I. Reconfigurable Knots and Links in Chiral Nematic Colloids. *Science* **2011**, *333*, 62-65.

(25) Martinez, A.; Ravnik, M.; Lucero, B.; Visvanathan, R.; Zumer, S.; Smalyukh, I. Mutually Tangled Colloidal Knots and Induced Defect Loops in Nematic Fields. *Nat. Mater.* **2014**, *13*, 258-263.

(26) Crawford, G. P.; Scharkowski, A.; Fung, Y. K.; Doane, J. W.; Zumer, S. Internal Surface, Orientational Order, and Distribution of a Polymer Network in a Liquid Crystal Matrix. *Phys. Rev. E.* **1995**, *52*, R1273-R1276.

(27) Miller, D. S.; Wang, X.; Abbott, N. L. Design of Functional Materials based on Liquid Crystalline Droplets. *Chem. Mater.* **2014**, *26*, 496-506.

(28) Noh, J.; Henx, B.; Lagerwall, J. P. F. Taming Liquid Crystal Self-Assembly: The Multifaceted Response of Nematic and Smectic Shells to Polymerization. *Adv. Mater.* **2016**, *28*, 10170-10174.

(29) Kikuchi, H.; Izena, S.; Higuchi, H.; Okumura, Y.; Higashiguchi, K. A Giant Polymer Lattice in a Polymer-Stabilized Blue Phase Liquid Crystal. *Soft Matter* **2015**, *11*, 4572-4575.

(30) Castles, F.; Day, F. V.; Morris, S. M.; Ko, D. H.; Gardiner, D. J.; Qasim, M. M.; Nosheen, S.; Hands, P. J. W.; Choi, S. S.; Friend, R. H.; Coles, H. J. Blue-Phase Templated Fabrication of Three-Dimensional Nanostructures for Photonic Applications. *Nat. Mater.* **2012**, *11*, 599-603.

(31) Kikuchi, H.; Yokota, M.; Hisakado, Y.; Yang, H.; Kajiyama, T. Polymer-Stabilized Liquid Crystal Blue Phases. *Nat. Mater.* **2002**, *1*, 64-68.

(32) Xiang, J.; Lavrentovich, O. D. Blue-Phase-Polymer-Templated Nematic with Sub-Millisecond Broad-Temperature Range Electro-Optic Switching. *Appl. Phys. Lett.* **2013**, *103*, 051112.

(33) Gleeson, H. F.; Liu, H.; Kaur, S.; Srigengan, S.; Gortz, V.; Mandle, R.; Lydon, J. E. Self-Assembling, Macroscopically Oriented, Polymer Filaments; a Doubly Nematic Organogel. *Soft Matter* **2018**, *14*, 9159-9167.

(34) Higashiguchi, K.; Yasui, K.; Ozawa, M.; Odoi, K.; Kikuchi, H. Spatial Distribution Control of Polymer Nanoparticles by Liquid Crystal Disclinations. *Polym. J.* **2012**, *44*, 632-638.

(35) Nagai, A.; Yoshii, R.; Otsuka, T.; Kokado, K.; Chujo, Y. BODIPY-Based Chain Transfer Agent: Reversibly Thermoswitchable Luminescent Gold Nanoparticle Stabilized by BODIPY-Terminated Water-Soluble Polymer. *Langmuir* **2010**, *26*, 15644-15649.

(36) Musevic, I.; Skarabot, M.; Tkalec, U.; Ravnik, M.; Zumer, S. Two-Dimensional Nematic Colloidal Crystals Self-Assembled by Topological Defects. *Science* **2006**, *313*, 954-958.

(37) Hoque, E.; DeRose, J. A.; Bhushan, B.; Mathieu, H. *Self-Assembled Monolayers on Aluminum and Copper Oxide Surfaces: Surface and Interface Characteristics, Nanotribological Properties, and Chemical Stability*; Tomitori, M.; Bhushan, B.; Fuchs, H., Eds.; Springer: Berlin, Heidelberg, **2008**; Chapter 10, pp 235-281.

(38) Mikhalyov, I.; Gretskaya, N.; Bergstrom, F.; Johansson, L. B. A. Electronic Ground and Excited State Properties of Dipyrrometheneboron Difluoride (BODIPY): Dimers with Application to Biosciences. *Phys. Chem. Chem. Phys.* **2002**, *4*, 5663-5670.

(39) Cladis, P. E.; Vansaarloos, W.; Finn, P. L.; Kortan, A. R. Dynamics of Line Defects in Nematic Liquid Crystals. *Phys. Rev. Lett.* **1987**, *58*, 222-225.

(40) Mullin, C. S.; Guyot-Sionnest, P.; Shen, Y. R. Properties of Liquid-Crystal Monolayers on Silane Surfaces. *Phys. Rev. A.* **1989**, *39*, 3745-3747.

(41) Kocevar, K.; Musevic, I. AFM Study of Forces in and Structures of Nematic Liquid Crystal Interfaces on Silanated Glass. *Liq. Cryst.* **2001**, *28*, 599-606.

(42) Xue, C.-Y.; Yang, K.-L. Dark-to-Bright Optical Responses of Liquid Crystals Supported on Solid Surfaces Decorated with Proteins. *Langmuir* **2008**, *24*, 563-567.

(43) Ruckenstein, E.; Nagarajan, R. Aggregation of Amphiphiles in Non-Aqueous Media. *J. Phys. Chem.* **1980**, *84*, 1349-1358.

(44) Wilber, A. W.; Doye, J. P. K.; Louis, A. A.; Noya, E. G.; Miller, M. A.; Wong, P. Reversible Self-Assembly of Patchy Particles into Monodisperse Icosahedral Clusters. *J. Chem. Phys.* **2007**, *127*, 085106.

(45) Nykypanchuk, D.; Maye, M. M.; van der Lelie, D.; Gang, O. DNA-Guided Crystallization of Colloidal Nanoparticles. *Nature* **2008**, *451*, 549-552.

(46) Becker, H. D. Unimolecular Photochemistry of Anthracenes. *Chem. Rev.* **1993**, *93*, 145-172.

(47) Canet-Ferrer, J.; Coronado, E.; Forment-Aliaga, A.; Pinilla-Cienfuegos, E. Correction of the Tip Convolution Effects in the Imaging of Nanostructures Studied through Scanning Force Microscopy. *Nanotechnology* **2014**, *25*, 395703.

(48) Chang, K.; Korovich, A.; Xue, T. Y.; Morris, W. A.; Madsen, L. A.; Geise, G. M. Influence of Rubbery versus Glassy Backbone Dynamics on Multiscale Transport in Polymer Membranes. *Macromolecules* **2018**, *51*, 9222-9233.

(49) Shi, H. F.; Zhao, Y.; Jiang, S. C.; Rottstegge, J.; Xin, J. H.; Wang, D. J.; Xu, D. F. Effect of Main-Chain Rigidity on the Phase Transitional Behavior of Comblike Polymers. *Macromolecules* **2007**, *40*, 3198-3203.

(50) Wind, M.; Graf, R.; Renker, S.; Spiess, H. W. Structural Reasons for Restricted Backbone Motion in Poly(n-Alkyl Methacrylates): Degree of Polymerization, Tacticity and Side-Chain Length. *Macromol. Chem. Phys.* **2005**, *206*, 142-156.

(51) Bates, W. W.; Hobbs, M. E. The Dipole Moments of Some Acid Amides and the Structure of the Amide Group. *J. Am. Chem. Soc.* **1951**, *73*, 2151-2156.

(52) Chow, L. C.; Martire, D. E. Thermodynamics of Solutions with Liquid Crystal Solvents .3. Molecular Interpretation of Solubility in Nematogenic Solvents. *J. Phys. Chem.* **1971**, *75*, 2005-2015.

(53) Yoshida, H.; Tanaka, Y.; Kawamoto, K.; Kubo, H.; Tsuda, T.; Fujii, A.; Kuwabata, S.; Kikuchi, H.; Ozaki, M. Nanoparticle-Stabilized Cholesteric Blue Phases. *Appl. Phys. Express* **2009**, *2*, 121501.

(54) Ravnik, M.; Alexander, G. P.; Yeomans, J. M.; Zumer, S. Three-Dimensional Colloidal Crystals in Liquid Crystalline Blue Phases. *Proc. Natl. Acad. Sci. U.S.A.* **2011**, *108*, 5188-5192.

(55) Fukuda, J. Stability of Cholesteric Blue Phases in the Presence of a Guest Component. *Phys. Rev. E.* **2012**, *86*, 041704.

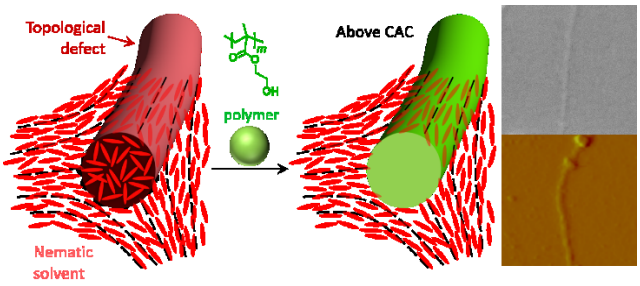

Table of Contents Artwork